PCCP
Physical Chemistry Chemical Physics

Accepted Manuscript

This article can be cited before page numbers have been issued, to do this please use: M. J. Mitchell, H. Ishkhanyan, M. Ulmschneider and C. D. Lorenz, *Phys. Chem. Chem. Phys.*, 2026, DOI: 10.1039/D5CP04113A.

View Article Online
DOI: 10.1039/D5CP04113A

Journal Name

ARTICLE TYPE

Cite this: DOI: 00.0000/xxxxxxxxxx

Drug-Dependent Modulation of Micelle Morphology and Encapsulation in Triton X-100 Systems†

Melissa Jade Mitchell,[a] Hrachya Ishkhanyan,[b,c], Martin B. Ulmschneider[d] and Christian D. Lorenz*[a,b,c]

Received Date
Accepted Date

DOI: 00.0000/xxxxxxxxxx

Micelle-based drug delivery systems offer a promising strategy for enhancing the solubility and bioavailability of poorly water-soluble therapeutics. Among these, nonionic surfactants such as Triton X-100 are particularly attractive due to their biocompatibility and capacity to encapsulate structurally diverse small molecules. In this work, all-atom molecular dynamics simulations were employed to investigate the encapsulation of three drugs (aspirin, atenolol, and felodipine) within Triton X-100 micelles. The selected molecules span a broad range of hydrophobicities and hydrogen-bonding capabilities, enabling a systematic comparison of how physicochemical properties influence solubilisation behaviour and micelle morphology.

The simulations reveal that drug–micelle interactions are dominated by the hydrophilic ethylene-oxide headgroups, with limited penetration into the hydrophobic core. Hydrophobicity correlates positively with total drug loading; however, deviations from this trend highlight the competing roles of polarity and conformational flexibility. Atenolol, the most polar compound, penetrates deepest into the micelle core and induces the greatest deformation, whereas felodipine's extended aromatic surface stabilises more spherical aggregates.

Overall, this work demonstrates that Triton X-100 micelles adapt dynamically to chemically diverse guest molecules. The results establish quantitative structure–property relationships linking molecular features, including hydrophobicity, polarity and topology, to encapsulation efficiency and micelle shape. These insights provide molecular-level understanding of the physicochemical principles governing solubilisation in nonionic micellar systems and support the broader application of molecular simulation as a predictive tool for micelle-based drug delivery formulations.

1 Introduction

Surfactants play a pivotal role in modern drug delivery system design due to their capacity to modulate key physicochemical properties of pharmaceutical formulations. Their amphiphilic nature allows them to interact effectively with both hydrophilic and hydrophobic components, facilitating improved solubility, bioavailability, and stability of drug compounds. These properties are particularly beneficial for hydrophobic drugs, where surfactants serve as solubilising agents by reducing interfacial tension and encapsulating drug molecules within micelles. Beyond solubility enhancement, surfactants contribute to controlled drug release, increased permeability across biological membranes, and even modulation of drug distribution and toxicity profiles. Some surfactants also exhibit intrinsic antimicrobial activity, which adds value by protecting formulations from microbial contamination. [1]

Among the array of surfactants utilised, nonionic types like Triton X-100 (TX-100) have garnered significant attention. TX-100 is either a nonionic surfactant known for its ability to self-assemble into micellar structures in aqueous environments [2,3], making it a promising candidate for enhancing the oral delivery of poorly water-soluble drugs [1,4]. Its molecular architecture comprises a hydrophilic polyethylene oxide chain and a bulky hydrophobic *p*-tert-octylphenyl group [5,6], allowing it to form micelles that can encapsulate hydrophobic drug molecules and improve their aqueous solubility [7].

[a] *Biological Physics and Soft Matter Group, Department of Physics, Faculty of Natural, Mathematical & Engineering Sciences, King's College London, London, WC2R 2LS, United Kingdom*
[b] *Computational Molecular Engineering Lab, Institute for Informatics and Automation Problems of the National Academy of Sciences of the Republic of Armenia, 1, P. Sevak str. Yerevan, Republic of Armenia*
[c] *Department of Engineering, Faculty of Natural, Mathematical & Engineering Sciences, King's College London, London, WC2R 2LS, United Kingdom*
[d] *Department of Chemistry, Faculty of Natural, Mathematical & Engineering Sciences, King's College London, London, SE1 1DB, United Kingdom*
* e-mail: chris.lorenz@kcl.ac.uk

† Supplementary Information available: Contact maps describing interactions of small molecular therapeutics with themselves and with the Triton X-100 surfactants. See DOI: 00.0000/00000000.

View Article Online
DOI: 10.1039/D5CP04113A

The critical micelle concentration (CMC) of Triton X-100 at 25 °C is typically reported between 0.2 and 0.31 mM, with slight variation depending on the experimental method and drug presence[5]. For instance, in the presence of nimesulide, the CMC has been determined to be approximately 0.25 mM[7]. Despite extensive study, the precise morphology of Triton X-100 micelles remains under discussion[8]. While traditional models depict a well-defined core-shell structure, more complex descriptions, featuring diffuse boundaries, multilayered configurations, and polydispersity, may more accurately represent their aggregation behavior[8]. The relatively short hydrophobic tail and the extended ethylene oxide chain may result in micelles with less distinct core-shell separation or favor oblate morphologies[8]. Molecular dynamics simulations further suggest that Triton X-100 micelles deviate from spherical geometry as their aggregation number increases[3,9,10].

A primary application of Triton X-100 micelles lies in enhancing the solubility and, consequently, the bioavailability of lipophilic drugs[2–4,11–14]. Hydrophobic drug molecules partition into the micellar core, while the hydrophilic shell interfaces with the aqueous environment[12]. This property has been explored using a variety of poorly water-soluble compounds. For example, nonsteroidal anti-inflammatory drugs (NSAIDs) such as ibuprofen and indomethacin have been extensively studied in Triton X-100 micellar systems. Triton X-100 micelles can significantly enhance the solubilisation of these agents, with indomethacin exhibiting approximately twice the solubility of ibuprofen at equivalent aggregation numbers. Indomethacin's tendency for π-π stacking leads to dense aggregation within the micelle core, which can cause micellar destabilisation and fission into smaller daughter micelles. In contrast, ibuprofen yields more stable, albeit elongated, micelles. Notably, Triton X-100 outperforms its TX-114 counterpart in solubilising ibuprofen[3,11]. Nimesulide has also been investigated, with UV–Vis spectroscopy indicating its incorporation into Triton X-100 micelles, although the interaction appears weaker than with cationic micelles[7]. Another example is syringic acid, whose partitioning into Triton X-100 micelles has provided further insight into the micellar encapsulation of bioactive phenolic compounds[4]. Beyond enhancing solubility, the nanoscale size (typically 5–100 nm) of micelles enables deeper tissue penetration, increased retention, and potentially enhanced cellular uptake via mechanisms such as transcytosis[12].

Triton X-100 holds promise in improving the oral delivery of poorly water-soluble drugs within drug delivery formulations by enhancing solubility and potentially influencing tissue permeability. Therefore, further investigation of the unique structural characteristics and dynamic aggregation behavior of Triton X-100 micelles, along with the interactions of various small molecule therapeutics, will be crucial in the further understanding of the mechanisms that result in the demonstrated solubilisation capacity of these micelles[5], which makes them a valuable platform for drug delivery research. In this manuscript, we have used all-atom molecular dynamics simulations to examine the interactions of three small molecule drugs (aspirin, atenolol, and felodipine) with Triton X-100 micelles. These drugs, selected for their differing bioavailability and hydrophobicity, provide a comparative framework to clarify how molecular properties affect micelle solubilisation. While previous molecular dynamics studies have provided valuable insight into the self-assembly and solubilisation mechanisms of Triton X-100 micelles, most have focused on individual drugs or on general micellar morphology without systematically relating molecular structure to encapsulation behaviour[3,8–11]. In contrast, the present work offers a comparative framework that directly examines how distinct physicochemical and structural features (e.g. aromaticity, polarity, and hydrogen-bonding capability) govern drug–micelle interactions under identical simulation conditions. By investigating three therapeutically relevant small molecules (aspirin, atenolol, and felodipine) that span a broad range of $\log P$ values and hydrogen-bond donor/acceptor profiles, we uncover how subtle variations in molecular topology influence encapsulation depth, micelle deformation, and interfacial hydration. This systematic, cross-drug comparison extends beyond prior work on single-drug systems and provides new molecular-level insights into how nonionic surfactant micelles accommodate chemically diverse cargo. These findings advance the physicochemical understanding of solubilisation in nonionic surfactant systems and contribute to establishing quantitative structure–property relationships that underpin drug encapsulation in aqueous micellar environments.

2 Methods

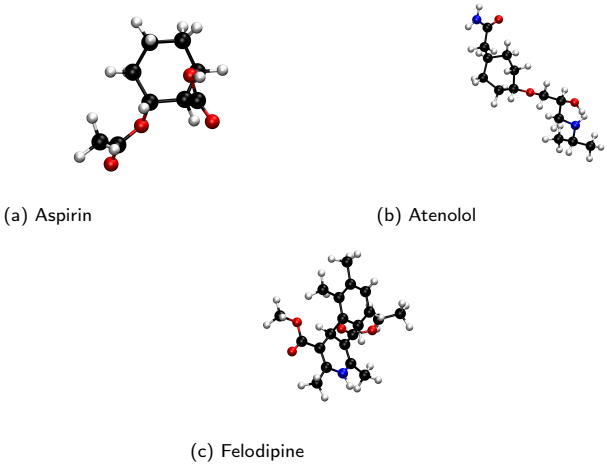

Fig. 1 Molecular representations of the three small-molecule drugs ((a) aspirin, (b) atenolol and (c) felodipine), with atoms colour-coded by element: carbon (black), oxygen (red), and nitrogen (blue). These representations are shown to indicate the three-dimensional conformation of each molecule as used in the simulations. The corresponding two-dimensional chemical structures, with explicit depiction of aromaticity and connectivity, are provided in Figure S3 of the Supporting Information.

All-atom molecular dynamics simulations were performed in this study using GROMACS version 2019.3[15] with the CHARMM36 force field[16] chosen to model the interactions between Triton X-100 micelles,water and small molecule drugs (Aspirin,Atenolol and Felodipine). The drug molecules were modelled and parameterised using Charmm-Gui PDB reader.

View Article Online
DOI: 10.1039/D5CP04113A

2.1 System Preparation

The pre-assembled Triton X-100 micelle used as the starting configuration in all three systems was taken directly from the equilibrated trajectory of our previous all-atom molecular dynamics study of TX-100 micelles loaded with ibuprofen and indomethacin[3]. In that study, a micelle of 150 TX-100 molecules was constructed using Packmol[17] and equilibrated under identical force field conditions (CHARMM36, CHARMM-modified TIP3P water[18,19], 310 K, 1.0 bar), resulting in a stable aggregate with an average aggregation number of 147 molecules. The use of this previously equilibrated micelle as the starting point ensures consistency with our prior work and avoids any dependence of the results on the initial self-assembly process. The drug molecules were subsequently inserted into the aqueous environment surrounding this micelle using the `gmx insert-molecules` tool, such that they were at least 1 nm from the micelle's surface. Water molecules were then added to fill the simulation box with dimensions of 130 Å × 130 Å × 130 Å for all systems.

2.2 Simulation Protocol

Energy minimisation was performed using the steepest descent algorithm with an energy tolerance of 1000.0 kJ/mol·nm and a maximum of 5000 steps. A Verlet cutoff scheme was applied, with a cutoff radius of 1.2 nm for Lennard-Jones interactions. Equilibration was carried out under NPT (constant number of particles, pressure, and temperature) conditions to relax the systems and achieve equilibrium. A Berendsen thermostat maintained the temperature at 310 K for all components (Triton X-100, water, and drug molecules) with a coupling time constant τ_t of 1.0 ps. Isotropic pressure coupling was applied using the Berendsen barostat with a reference pressure of 1.0 bar, a time constant τ_p of 5.0 ps. Production simulations were conducted under NPT conditions for 1 microsecond per system to capture the dynamics of drug-micelle interactions. The Nose-Hoover thermostat was used for temperature control, maintaining a stable temperature of 310 K with $\tau_t = 1.0$ ps. Isotropic pressure coupling was achieved using the Parrinello-Rahman barostat with a reference pressure of 1.0 bar, $\tau_p = 5.0$ ps, and compressibility of $4.5 \times 10^{-5}\,\mathrm{bar}^{-1}$.

To verify that the 0.5 ns equilibration period was sufficient to achieve equilibrium prior to the production simulations, we monitored the time evolution of the radius of gyration and the ellipticity of the Triton X-100 micelle for each system. Both quantities undergo an initial relaxation, after which they converge to stable, fluctuating values with no systematic drift observed over the remainder of the equilibration trajectory. This indicates that both the micellar core dimensions and the overall micelle shape had reached a stable equilibrium prior to the commencement of the production simulations (see Figure S4).

3 Data Analysis

3.1 Interface

The hydrophobic core of the micelle was defined geometrically in each trajectory frame by constructing a convex hull around the head group atoms of TX-100 (atoms C19, C20, C21, C22, C23, C24). The core radius was calculated as the mean distance from the centre of mass of all of the TX-100 atoms to the convex hull, averaged across all trajectory frames. The interface of the entire micelle was defined equivalently using a convex hull around all TX-100 atoms.[20]

3.2 Hydration

To calculate the hydration of the drug molecules, a radial distribution function (RDF) was used to define the probability that the oxygen atom in a water molecule (Ow) is found at a given distance from the polar oxygen atoms (Ox) within the small molecules (for aspirin, atenolol and felodipine, atoms 01, 02, 03 and 04[21]. The radial distribution function $g_{Ox,Ow}(r)$ is formulated as:

$$g_{Ox,Ow}(r) = \frac{\rho_{Ox,Ow}(r)}{\langle \rho_{Ow} \rangle} \tag{1}$$

In this equation, $\rho_{Ox,Ow}(r)$ signifies the density of oxygen atoms in the water molecules situated at a distance r from atoms of type Ox. Meanwhile, $\langle \rho_{Ow} \rangle$ represents the mean density of the oxygen atoms in the water molecules.

The first neighbour distance is defined as the distance at which the first minimum after the first peak of the RDF occurs. The number of water molecules in the first hydration shell of each of these polar atoms is then determined by counting the number of water molecules that are found within the first neighbour distance of each oxygen and averaging over the number of drug molecules and over time.

3.3 Density

The density distributions of each molecular species present in the system were computed using the PUCHIK package[20]. PUCHIK fits an alpha shape surface to the micelle's hydrophobic core and then bins the atomic positions as a function of signed distance from this intrinsic water-core interface.

3.4 Encapsulation

The encapsulation efficiency of drug molecules within the micelle (E) was evaluated by counting the number of drug molecules located within the micelle's core. To calculate the core, we identified the center of mass of the Triton X-100 micelles using the selected head groups[22].

$N_{\mathrm{encapsulated}}$ and dividing it by the total number of drugs in the simulation N_{total}:

$$E = \frac{N_{\mathrm{encapsulated}}}{N_{\mathrm{total}}} \times 100. \tag{2}$$

E was calculated for each configuration within the trajectory.

3.5 Micelle Shape Analysis

To characterise the shape of the micelle, we calculated the principal moments of inertia from the positions of the micelle's convex hull points. The convex hull is the smallest convex boundary that encloses a set of points. Using coordinates of these hull points it helps to calculate the moments of inertia[3].

The moments of inertia I were computed as:

View Article Online
DOI: 10.1039/D5CP04113A

$$I_x = \sum_i \left(y_i^2 + z_i^2\right), \quad I_y = \sum_i \left(x_i^2 + z_i^2\right), \quad I_z = \sum_i \left(x_i^2 + y_i^2\right) \qquad (3)$$

where x_i, y_i, and z_i are the coordinates of the convex hull points relative to the micelle's center of mass. The eigenvalues of the inertia tensor were used to classify the micelle's shape as spherical, prolate, oblate or triaxial.

There are different methods to help determine the shape of the micelle based on the ratios of the principal moments of inertia. Let the three principal moments be ordered as $I_1 \leq I_2 \leq I_3$. The micelle shape is classified as spherical when all three moments are approximately equal (within 5% deviation), prolate when $I_1 \approx I_2 < I_3$ (with the two smaller moments differing by less than 10% while being at least 15% smaller than the largest), and oblate when $I_1 < I_2 \approx I_3$ (with the two larger moments differing by less than 10% while being at least 15% greater than the smallest). If none of these criteria are met, the shape is classified as triaxial[23].

4 Results and discussion

4.1 Structural properties of Triton X-100 drug delivery vehicles

In Figure 2, the distance axis is defined relative to the intrinsic surface of the hydrophobic core of the micelle, as calculated using the convex hull construction described in the Methods section. A distance of 0 Å corresponds to the convex hull surface itself; negative values indicate positions within the hydrophobic core interior, and positive values indicate positions within the hydrophilic corona or the surrounding aqueous phase. The intrinsic density profiles shown in Figure 2 provide insight into the internal and interfacial structure of the Triton X-100 micelles loaded with the various drugs. In each micelle, we find that the significant majority of the hydrophobic tails of the Triton X-100 surfactants are within the core of the micelle. While the ethylene oxide chains that form the hydrophilic head groups of surfactant molecules do penetrate the core of the micelles, which we have seen in our previous studies as well[11,24], they are generally found interacting with the aqueous environment of the micelles.

The three different small molecule therapeutics are generally found at the interface of the hydrophobic core of the micelle, but they are found to penetrate the hydrophobic core of the micelles to varying degrees. The felodipine molecules are found to penetrate a bit more than aspirin, while atenolol does not penetrate deep into the hydrophobic core; instead, its density is concentrated at the core–corona interface, consistent with its low $\log P$ value.

The general density profile of the water surrounding the micelles is consistent for all three micelles. The density of the water begins to decrease from the bulk density at a distance of ~ 18 Å from the interface of the hydrophobic core of the micelle, which corresponds to the maximum extent of the hydrophilic head groups of the Triton X-100 molecules within the micelle. The density of the water continues to decrease linearly as the density of the hydrophilic head groups of surfactants increases nearer to the interface of the core of the micelle. Water is found to be present within the core of each micelle, with water penetrating the micelle that has encapsulated aspirin the most, followed by the micelle with atenolol.

Table 1 reports the size and shape of the Triton X-100 micelles loaded with the three different small molecule therapeutics. It is clear from these results that the encapsulation of the different drugs affects the structure of the micelles in different ways. The volumes of the three drug-loaded micelles are 80.3 ± 3.3 nm^3 (aspirin), 80.7 ± 1.5 nm^3 (atenolol), and 78.5 ± 3.0 nm^3 (felodipine). While the mean volume is marginally larger for the atenolol-loaded system, the difference between the atenolol and aspirin systems (0.4 nm^3) is smaller than the standard deviation of either measurement and is therefore not statistically significant. In contrast, the felodipine-loaded micelle has a measurably smaller volume than the atenolol-loaded micelle, consistent with the more compact, spherical packing induced by felodipine's extended hydrophobic surface area. The ellipticity values, which are more sensitive indicators of morphological change, show a clearer trend: the atenolol-loaded micelle (3.8 ± 0.2) is substantially more aspherical than the aspirin-loaded (1.9 ± 0.3) and felodipine-loaded (1.6 ± 0.1) systems. However, the overall shape of all three drug-loaded micelles, as determined by the moments of inertia, is the same (triaxial).

4.2 Solubilisation of small molecule therapeutics within Triton X-100 micelles

The solubilisation dynamics of aspirin, atenolol, and felodipine in Triton X-100 micelles (Fig. 3) provide insight into the interactions between each of the small molecule drugs and the micelles. Generally, we observe that initially the drug molecules prefer to be solubilised within the hydrophilic corona of the micelle as the number of drug molecules solubilised within the whole micelle (which counts those within the corona and within the hydrophobic core) is larger from the very start of the analysed simulations than the number in the core of the micelle. The encapsulation of drugs within the hydrophobic core proceeds at different rates for each therapeutic. For aspirin, core occupancy reaches a plateau of $\sim$22 molecules reached at approximately $t = 750$ ns, after which the count remains stable for the remainder of the simulation. Atenolol reaches a similar plateau value of $\sim$35 molecules by approximately $t = 900$ ns, whereas felodipine, reaches a stable plateau at approximately $t = 600$ ns. The equilibration of the total micelle occupancy and core occupancy, which occur over the same time scales, indicates that the partitioning of all three drugs between the corona, core, and bulk aqueous phase has reached a dynamic steady state over the timescale of the simulation.

As a result, the number of drugs solubilised within the hydrophobic core of the micelle and within the total micelle equilibrates after approximately 600 ns. As summarised in Table 1, the Triton X-100 micelle is able to encapsulate more atenolol within its hydrophobic core (35 ± 2.6 molecules) than either felodipine (28 ± 1.7) or aspirin (22 ± 1.9).

The elevated $n_{e,\text{core}}$ value for atenolol (35 ± 2.6) relative to felodipine (28 ± 1.7) and aspirin (22 ± 1.9) may appear counter-intuitive given atenolol's low hydrophobicity ($\log P = 0.16$). How-

View Article Online
DOI: 10.1039/D5CP04113A

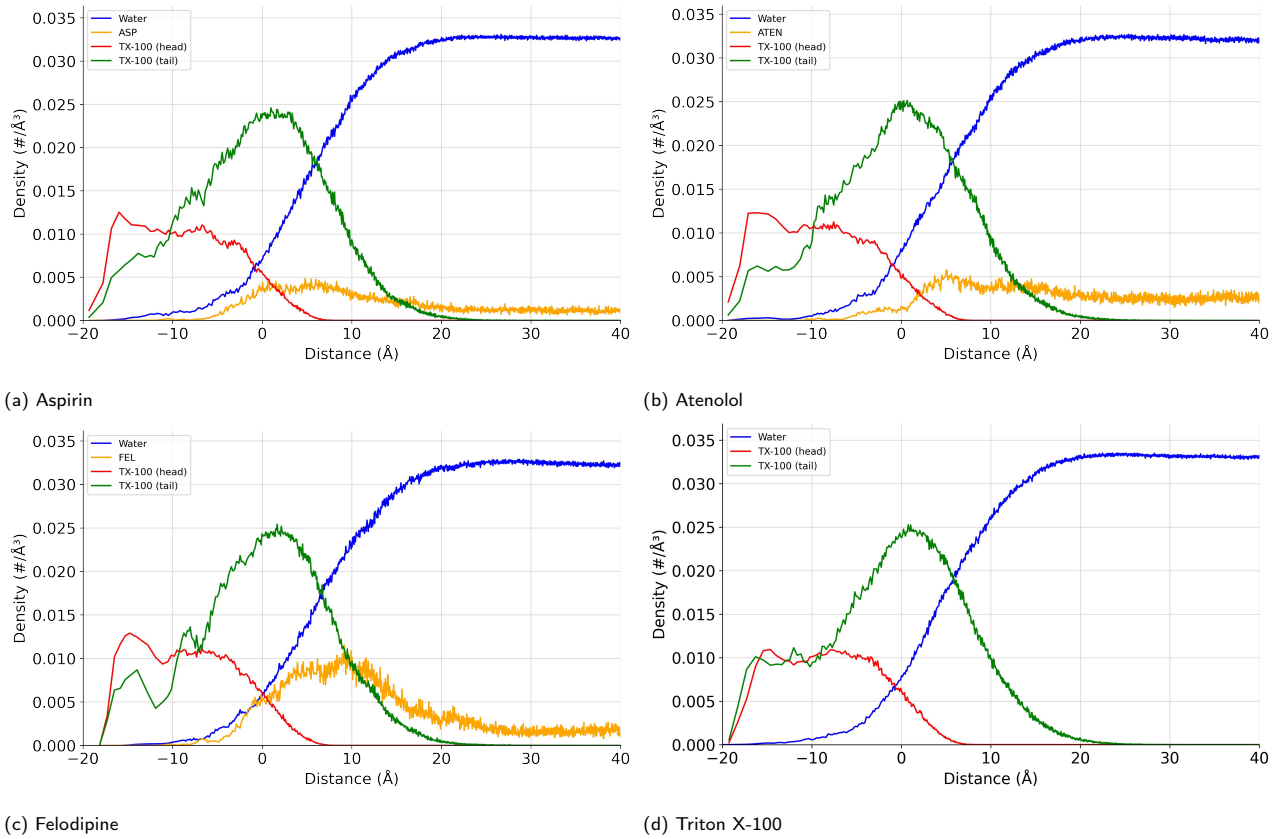

Fig. 2 Density profiles of small molecule drugs within Triton X-100 micelles. The density of the oxygen atoms in the water molecules (blue), the carbon atoms in the hydrophobic tail (green) and hydrophilic head (red) groups of the Triton X-100 surfactant molecules, and each small molecule drug ((a) aspirin, (b) atenolol and (c) felodipine) (orange) is plotted as a function of distance from the interface of the hydrophobic core of the micelle. Panel (d) shows the corresponding density profile for the neat Triton X-100 micelle in the absence of any drug, reproduced from Ishkhanyan et al.[3] under a Creative Commons Attribution 3.0 licence (CC BY 3.0), and is provided as a structural reference against which the effect of drug loading on the internal organisation of the micelle can be assessed.

ever, this reflects the geometric definition of the core boundary: molecules residing at the convex hull surface of the hydrophobic core are counted as encapsulated within it. Atenolol, being insufficiently hydrophobic to partition into bulk water yet too polar to penetrate the hydrophobic interior, accumulates preferentially at this interface. This interfacial localisation is confirmed by the density profiles in Figure 2, where the atenolol density peaks sharply at the core boundary (distance $= 0$ Å) with negligible density at negative distances corresponding to the hydrophobic interior. The high $n_{e,\mathrm{core}}$ value therefore reflects a large interfacial surface excess rather than genuine penetration into the hydrophobic core, consistent with the thermodynamic expectation that strongly polar molecules partition to the most energetically accessible region of the micelle — in this case the core–corona interface, where atenolol can simultaneously avoid the hydrophobic interior while hydrogen bonding with the ethylene oxide headgroups of the Triton X-100 surfactants that coat the core boundary.

While when accounting for the number of drug molecules solubilised within the hydrophilic headgroups of the surfactant molecules, the micelle is found to encapsulate more felodipine (66 ± 2.0 molecules) than either aspirin (57 ± 2.5) or atenolol (53 ± 1.9). The observed trends in the number of drugs encapsulated in the entirity of the micelles is consistent with trend observed in the $\log P$ values of each small molecule (Table 1).

4.3 Internal structure of drug-loaded Triton X-100 micelles

Figures 4 & S1 shows the contact maps that describe the interactions which govern any aggregation of the small molecule therapeutics. A contact between two atoms was defined as a distance of 5Å between any two non-hydrogen atoms. In general we find that both aspirin and atenolol prefer to interact via their phenyl rings. The carboxyl group is also found to be involved in the interactions between aspirin molecules. Meanwhile felodipine molecules generally interact via the carbons in its pyridine ring and the methyl groups that are attached to the pyridine ring.

The interactions between the small molecule therapeutics and the Triton X-100 molecules that encapsulate them have also been investigated (Figures 5 & S2). Interestingly, all the small molecules are most commonly found to interact with the hydrophilic head groups of the Triton X-100 surfactants. The small molecules interact with the ethylene oxide groups within these head groups when they are encapsulated in the corona of the micelles, as they move to the hydrophobic core of the micelle and when they are at the interface of this core, which the hydrophilic groups of the Triton X-100 surfactants also coat to some degree

View Article Online
DOI: 10.1039/D5CP04113A

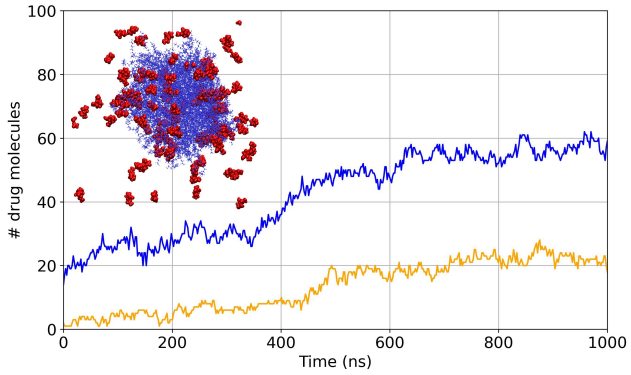

(a) Aspirin

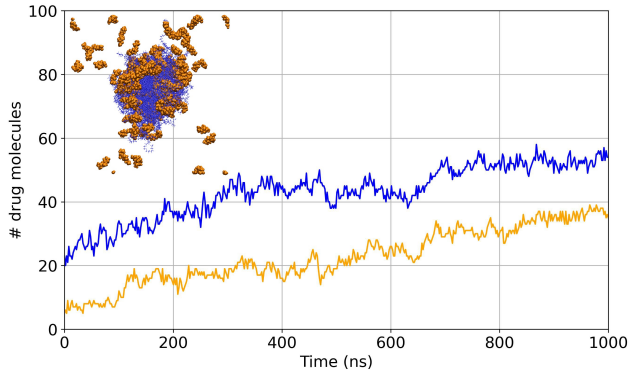

(b) Atenolol

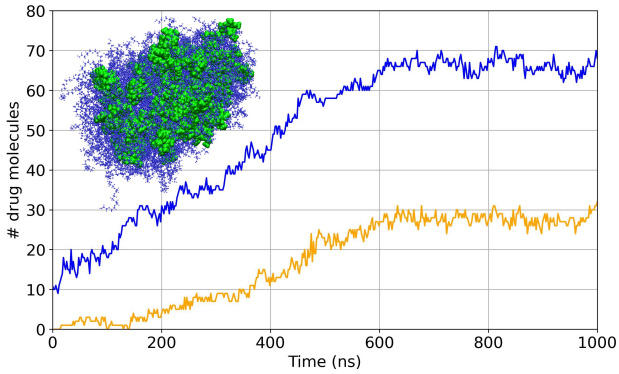

(c) Felodipine

Fig. 3 Solubilisation of small molecule drugs within Triton X-100 micelles. Each figure shows the number of drug molecules ((a) aspirin, (b) atenolol & (c) felodipine) that have been solubilised within the entire Triton-X 100 micelle (blue) and within the hydrophobic core (orange) as a function of time.

View Article Online
DOI: 10.1039/D5CP04113A

Property	Aspirin	Atenolol	Felodipine	Pure Triton X-100
n_{agg}	150	144	150	147
Radius of Gyration (nm)	3.1 ± 1.2	3.9 ± 1.0	3.2 ± 0.3	–
Surface Area (nm^2)	101.1 ± 2.5	101.7 ± 1.8	103.6 ± 2.3	
Volume (nm^3)	80.4 ± 2.8	81.2 ± 1.9	79.6 ± 2.4	–
Ellipticity	1.8 ± 0.3	4.2 ± 0.3	1.6 ± 0.1	1.48
Shape	Triaxial	Triaxial	Triaxial	Prolate
$n_{e,total}$	57 ± 2.5	53 ± 1.9	66 ± 2	–
$n_{e,core}$	22 ± 1.9	35 ± 2.6	28 ± 1.7	–
$\log P$	1.19[25]	0.16[25]	4.46[26]	–

Table 1 Properties of Triton X-100 drug delivery vehicles. $n_{e,total}$ and $n_{e,core}$ are the average number of each of the small molecule therapeutics that we find encapsulated in the whole micelle and within the hydrophobic core, as defined with our intrinsic surface calculations, of the micelle. [Note: The values for the properties of the pure Triton X-100 micelle (Pure Triton X-100) were taken from previously published work. [3]]

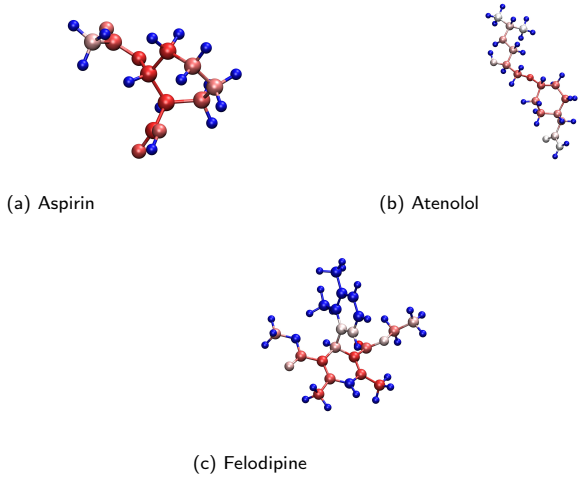

(a) Aspirin (b) Atenolol

(c) Felodipine

Fig. 4 Interactions between small molecule therapeutics. Atomistic structures coloured by the amount of contact with an atom in each of the small molecule therapeutics: (a) aspirin, (b) atenolol, and (c) felodipine). A contact event is defined as any pair of non-hydrogen atoms from different molecules separated by a distance of less than 5 Å. The contact frequency for each atom is computed as the fraction of trajectory frames (sampled over the 1 μs production simulation) in which that atom participates in at least one such contact. Red represents a high contact frequency (approaching 1.0), blue represents a low contact frequency (approaching 0.0), and white represents intermediate values.

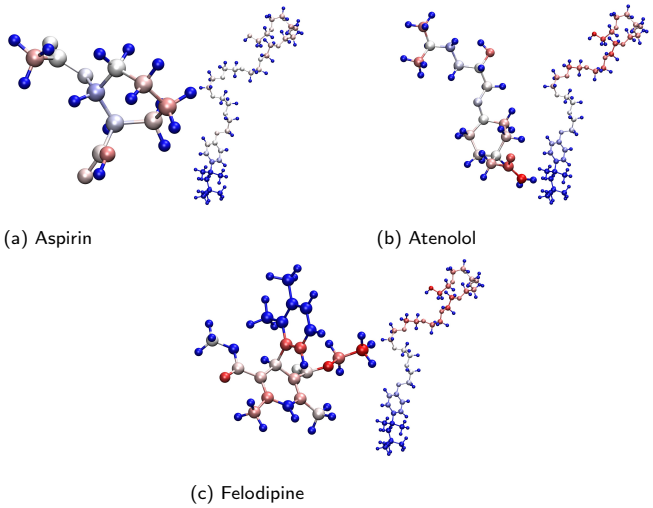

(a) Aspirin (b) Atenolol

(c) Felodipine

Fig. 5 Interactions between small molecule therapeutics and the Triton X-100 surfactants. Atomistic structures coloured by the amount of contact showing the interactions between the Triton X-100 surfactants and the small molecule therapeutics. A contact event is defined as any pair of non-hydrogen atoms from different molecules separated by a distance of less than 5 Å. The contact frequency for each atom is computed as the fraction of trajectory frames (sampled over the 1 μs production simulation) in which that atom participates in at least one such contact. Red represents a high contact frequency (approaching 1.0), blue represents a low contact frequency (approaching 0.0), and white represents intermediate values.

View Article Online
DOI: 10.1039/D5CP04113A

to stablise the micelles in an aqueous environment.

Atenolol does not form strong interactions with the hydrophobic tails of the surfactant molecules. Meanwhile, aspirin and felodipine appear to form interactions with the benzene rings within the Triton X-100 molecules. As none of the small molecules are found to be present deep within the hydrophobic core of the micelles, it is not surprising that there is limited interactions with the hydrophobic tails of the surfactants, which would be found in the core of the micelles.

The regions of the small molecules that were found to interact with the Triton X-100 molecules are different from those that were found to be important in the aggregation of the small molecules. Both aspirin and atenolol form a significant proportion of their interactions with the surfactants between -OH groups that form hydrogen bonds with the oxygens in the ethylene groups in the hydrophilic headgroups of Triton X-100.

5 Conclusion

This study leveraged all-atom molecular dynamics simulations to elucidate the molecular determinants of drug encapsulation within Triton X-100 micelles. Through a comparative analysis of three therapeutically relevant small molecules (aspirin, atenolol, and felodipine) we show that the interplay between hydrophobicity, polarity, and molecular topology governs both encapsulation efficiency and micelle morphology. Hydrophobicity, expressed through the $\log P$ value, correlates positively with overall loading, yet deviations from this trend, particularly the deeper encapsulation of the more polar atenolol, reveal the important role of hydrogen bonding and conformational flexibility in driving localisation within the micelle interior.

Micelles loaded with atenolol exhibit the largest ellipticity, indicating that asymmetric hydrogen bonding at the interface promotes anisotropic deformation. In contrast, felodipine's compact, hydrophobic structure and extended aromatic surface area favour strong van der Waals interactions with the alkyl and aromatic regions of the surfactant, stabilising more spherical micelles. These results demonstrate that micelle morphology adapts dynamically to accommodate chemically diverse guests, with shape anisotropy and internal hydration emerging as sensitive indicators of molecular compatibility between drug and carrier.

By linking atomistic interaction patterns to mesoscopic micelle properties, this work provides a molecular-scale framework for understanding the physicochemical factors that control solubilisation and morphological adaptation in nonionic surfactant aggregates. These insights help establish quantitative structure–property relationships for drug–micelle systems, supporting the broader use of molecular simulation as a predictive tool in the rational formulation of aqueous micellar carriers.

From a practical perspective, the quantitative structure–property relationships established here offer actionable guidance for the rational formulation of nonionic micellar drug delivery systems. For hydrophobic drugs with high $\log P$ values, such as felodipine, the results indicate that Triton X-100 micelles provide efficient total loading via partitioning into the hydrophilic corona, while maintaining a more spherical, stable morphology. This is advantageous where colloidal stability is a primary formulation objective. For polar drugs with low $\log P$ values, such as atenolol, the preferential accumulation at the core–corona interface suggests that micellar encapsulation may still offer a solubilisation benefit, albeit through a different structural mechanism — one driven by interfacial hydrogen bonding rather than hydrophobic partitioning. The observation that atenolol induces the greatest micelle deformation has implications for the long-term stability of such formulations, as highly aspherical aggregates may be more susceptible to structural rearrangement or disassembly. These findings therefore suggest that the selection of a micellar carrier should account not only for the hydrophobicity of the drug but also for the sensitivity of the micellar morphology to guest-induced deformation. More broadly, this work demonstrates that all-atom molecular dynamics simulation can serve as a cost-effective, high-resolution predictive tool for screening drug–surfactant compatibility prior to experimental formulation, thereby accelerating the rational design of micellar delivery vehicles for chemically diverse therapeutics.

Author contributions

Conceptualization: Hrachya Ishkhanyan, Christian D. Lorenz; Data curation: Melissa Jade Mitchell; Formal analysis: Melissa Jade Mitchell; Investigation: Melissa Jade Mitchell; Methodology: Melissa Jade Mitchell, Hrachya Ishkhanyan, Christian D. Lorenz; Project administration: Christian D. Lorenz; Resources: Christian D. Lorenz; Software: Melissa Jade Mitchell, Hrachya Ishkhanyan; Supervision: Martin B. Ulmschneider, Christian D. Lorenz; Validation: Melissa Jade Mitchell; Visualization: Melissa Jade Mitchell; Writing – original draft: Melissa Jade Mitchell, Christian D. Lorenz; Writing – review & editing: Melissa Jade Mitchell, Hrachya Ishkhanyan, Christian D. Lorenz.

Conflicts of interest

There are no conflicts to declare.

Data availability

The files required to perform the simulations, the initial and final configurations of the various systems as well as the scripts that were used to analyse the simulations and therefore produce the data reported in this manuscript can be found on the Lorenz Lab github page (Lorenz Lab Github).

Acknowledgements

We are grateful to the UK Materials and Molecular Modelling Hub for computational resources, which is partially funded by EPSRC (EP/T022213/1, EP/W032260/1 and EP/P020194/1). We also appreciate the King's Computational Research, Engineering and Technology Environment (CREATE) at King's College London for providing us access to computational resources[27]. C. D. L. and H. I. acknowledge the Higher Education and Science Committee of the Republic of Armenia for supporting this research (Grant No. N 24RL-1C009). M. J. M., M. B. U. and C. D. L. acknowledge the support from the Biological Physics Across Scales Centre for Doctoral Training, funded by King's College London.

View Article Online
DOI: 10.1039/D5CP04113A

References

1 N. Chhetri and M. Ali, *J. Mol. Liq.*, 2023, **382**, 121858.

2 J. Lalthlengliani, J. Gurung and A. K. Pulikkal, *J. Mol. Liq.*, 2022, **354**, 118823.

3 H. Ishkhanyan, N. H. Rhys, D. J. Barlow, M. J. Lawrence and C. D. Lorenz, *Nanoscale*, 2022, **14**, 5392–5403.

4 Tinku, P. Gautam and S. Choudhary, *Journal of Molecular Liquids*, 2024, **398**, 123744.

5 A. Jahan and S. M. Nuruzzaman, *ChemistrySelect*, 2025, **10**, e202403158.

6 S. A. Maya, I. Jahan, J. M. Khan, S. M. A. Ahsan, S. Rana, M. M. Rahman, M. A. Hoque, M. A. Goni and M. A. Khan, *Journal of Solution Chemistry*, 2024, **53**, 1527–1543.

7 M. Enache, B. M. Andriesei, A. Oancea and S. Avram, *J. Mol. Liq.*, 2023, **392**, 123511.

8 H. M. Cezar, V. A. Bjørnestad, S. Prévost, R. Lund and M. Cascella, *Small Struct.*, 2024, **5**, 2400553.

9 A. D. Nicola, T. Kawakatsu, C. Rosano, M. Celino, M. Rocco and G. Milano, *J. Chem. Theory Comput.*, 2015, **11**, 4959–4971.

10 W. Murakami, A. D. Nicola, Y. Oya, J.-I. Takimoto, M. Celino, T. Kawakatsu and G. Milano, *ACS Appl. Nano Mater.*, 2021, **4**, 4552–4561.

11 H. Ishkhanyan, R. M. Ziolek, D. Barlow, J. Lawrence, A. H. Poghosyan and C. D. Lorenz, *J. Mol. Liq.*, 2022, **356**, 119050.

12 B. Homayun, X. Lin and H. J. Choi, *Pharmaceutics*, 2019, **11**, 129.

13 T. Hasan, M. J. Uddin, F. M. Efaz, J. M. Khan, S. Rana, M. A. Hoque, M. A. Halim and M. M. Rahman, *J. Mol. Liq.*, 2024, **407**, 125128.

14 F. Ahmad, M. Usman, A. Rauf, S. Nawaz, L. Rasool, U. Shafqat, A. Yusaf and N. Rasool, *Colloids Surf. A: Physicochem. Eng. Asp*, 2024, **687**, 133467.

15 M. Abraham, T. Murtola, R. Schulz, S. Páll, J. Smith, B. Hess and E. Lindahl, *SoftwareX*, 2015, **1–2**, 19–25.

16 S. Kim, J. Lee, S. Jo, C. L. Brooks, H. S. Lee and W. Im, *J. Comput. Chem.*, 2017, **38**, year.

17 L. Martínez, R. Andrade, E. G. Birgin and J. M. Martínez, *J. Comput. Chem.*, 2009, **30**, 2157–2164.

18 E. Neria, S. Fischer and M. Karplus, *J. Chem. Phys.*, 1996, **105**, 1902–1921.

19 J. A. D. MacKerell, D. Bashford, M. Bellott, J. R. L. Dunbrack, J. D. Evanseck, M. J. Field, S. Fischer, J. Gao, H. Guo, S. Ha, D. Joseph-McCarthy, L. Kuchnir, K. Kuczera, F. T. K. Lau, C. Mattos, S. Michnick, T. Ngo, D. T. Nguyen, B. Prodhom, I. W. E.Ñeiher, B. Roux, M. Schlenkrich, J. C. Smith, R. Stote, J. Straub, M. Watanabe, J. Wiórkiewicz-Kuczera, D. Yin and M. Karplus, *J. Phys. Chem. B*, 1998, **102**, 3586–3616.

20 H. Ishkhanyan, A. Santana-Bonilla and C. D. Lorenz, *J. Chem. Inf. Model.*, 2025, **65**, 1694–1701.

21 M. T. McDonnell, D. A. Greeley, K. M. Kit and D. J. Keffer, *J. Phys. Chem. B*, 2016, **120**, 8997–9010.

22 M. Z. Dehaghani, F. Yousefi, F. Seidi, B. Bagheri, A. H. Mashhadzadeh, G. Naderi, A. Esmaeili, O. Abida, S. Habibzadeh, M. R. Saeb and M. Rybachuk, *Sci. Rep.*, 2021, **11**, 18753.

23 K. Watanabe and M. L. Klein, *J. Phys. Chem.*, 1989, **93**, 6897–6901.

24 R. M. Ziolek, P. Smith, D. L. Pink, C. A. Dreiss and C. D. Lorenz, *Macromolecules*, 2021, **54**, 3755–3768.

25 A. Pyka-Pająk and M. B. Zachariasz, *Acta Pol. Pharm.*, 2006, **63**, 159–167.

26 R. van der Lee, M. Pfaffendorf, R. P. Koopmans, J. J. van Lieshout, G. A. van Montfrans and P. A. van Zwieten, *Blood Press.*, 2001, **10**, 217–222.

27 e Research, *King's Computational Research, Engineering and Technology Environment (CREATE)*, 2025, `https://doi.org/10.18742/rnvf-m076`.

View Article Online
DOI: 10.1039/D5CP04113A

Data availability statement

The files required to perform the simulations, the initial and final configurations of the various systems as well as the scripts that were used to analyse the simulations and therefore produce the data reported in this manuscript can be found on the Lorenz Lab github page .